AIP | Applied Physics Letters

Using coupled micropillar compression and micro-Laue diffraction to investigate deformation mechanisms in a complex metallic alloy Al13Co4

Ayan Bhowmik, Igor P. Dolbnya, T. Ben Britton, Nicholas G. Jones, Giorgio Sernicola, Claudia Walter, Peter Gille, David Dye, William J. Clegg, and Finn Giuliani

Citation: Applied Physics Letters **108**, 111902 (2016); doi: 10.1063/1.4944486
View online: http://dx.doi.org/10.1063/1.4944486
View Table of Contents: http://scitation.aip.org/content/aip/journal/apl/108/11?ver=pdfcov
Published by the AIP Publishing

Using coupled micropillar compression and micro-Laue diffraction to investigate deformation mechanisms in a complex metallic alloy $Al_{13}Co_4$

Ayan Bhowmik,[1,a)] Igor P. Dolbnya,[2] T. Ben Britton,[1] Nicholas G. Jones,[3] Giorgio Sernicola,[1] Claudia Walter,[3] Peter Gille,[4] David Dye,[1] William J. Clegg,[3] and Finn Giuliani[1,5]
[1]*Department of Materials, Imperial College London, Exhibition Road, London SW7 2AZ, United Kingdom*
[2]*Diamond Light Source, Didcot, Oxfordshire OX11 0DE, United Kingdom*
[3]*Department of Materials Science and Metallurgy, University of Cambridge, Cambridge CB3 0FS, United Kingdom*
[4]*Crystallographic Section, Department of Earth and Environmental Sciences, Ludwig-Maximilians-Universität München, Munich D-80333, Germany*
[5]*Department of Mechanical Engineering, Imperial College London, London SW7 2AZ, United Kingdom*

(Received 18 January 2016; accepted 2 March 2016; published online 17 March 2016; corrected 18 March 2016)

In this study, we have used *in-situ* micro-Laue diffraction combined with micropillar compression of focused ion beam milled $Al_{13}Co_4$ complex metallic alloy to investigate the evolution of deformation in $Al_{13}Co_4$. Streaking of the Laue spots shows that the onset of plastic flow occurs at stresses as low as 0.8 GPa, although macroscopic yield only becomes apparent at 2 GPa. The measured misorientations, obtained from peak splitting, enable the geometrically necessary dislocation density to be estimated as $1.1 \times 10^{13}\,m^{-2}$. © *2016 AIP Publishing LLC*. [http://dx.doi.org/10.1063/1.4944486]

$Al_{13}Co_4$ is a complex metallic alloy (CMA) with a unit cell of 102 atoms. The orthorhombic form has a unit cell with lattice parameters of $\mathbf{a} = 8.158$ Å, $\mathbf{b} = 12.342$ Å, and $\mathbf{c} = 14.452$ Å.[1] These alloys are brittle in nature and bulk plastic deformation is only possible at temperatures in excess of 600 °C.[2] During plastic deformation these materials show localised zones of inhomogeneous deformation characterised by extensive planar faults, which are bounded by dislocations with a [010] Burgers vector.[2] These are partial dislocations, called "meta-dislocations" with extended cores over the (001)-glide plane, and being partials they leave behind trailing faults.[3–5] Recently, the movement of metadislocations has been proposed to take place by jumps of both Co and Al atoms. Therefore, a glide step of nearly one unit cell (12.3 Å) can form by rearrangement of large number of atoms in the dislocation core.[6] Looking down the [100]-direction using high resolution scanning transmission electron microscopy the core of a dislocation is found to be made up of either four, six, or ten stacking faults.[7] A small length-scale study on $Al_{13}Co_4$ micropillars, focusing on slip on individual slip systems was carried out using micropillar compression from room temperature up to 600 °C.[8] Although such micropillars were found to be stronger than bulk material, the slip patterns remained similar over the test temperature range, being made up of mainly planar faults and dislocations.[8]

So far, understanding deformation in orthorhombic-$Al_{13}Co_4$ has been based on microstructural observation following deformation. The use of *in-situ* testing strategies enables confirmation of post-mortem observations, as well as understanding the progression of deformation in these materials. The combination of micropillar deformation and micro-Laue diffraction is attractive as it enables characterisation of changes in microstructure during deformation in real time, with through-thickness observations of the evolution of internal microstructure.[9] The use of micro Laue diffraction allows obtaining information from the entire volume of the micropillar rather than just surface characterisation and the use of a "white" x-ray beam enables probing the development of rotational and strain gradients in both polycrystal[10–12] and single crystals.[13–17] This technique has been employed to understand deformation in terms of sequential activation of several slip systems, in various pure metals like Si,[14] Au,[14] Mo,[15] Cu,[16] and W.[17] In Laue diffraction, the position and energy of the Laue spots is dependent on the orientation of the crystal and lattice parameters; however, typical studies do not measure the energy of the diffracted spots and so the technique is usually insensitive to hydrostatic strain. In plastic deformation, changes in the crystal orientation and lattice strain gradients within the illuminated volume correspond to activation of particular slip plane and continued slip on the given plane, respectively.[18,19] For example, this approach has been employed to study evolution of strain in second phase precipitates of zirconium hydride embedded within Zr-rich matrix.[20] In the present study, we combine *in-situ* micro-Laue diffraction with compressive loading of micropillars to capture different stages of deformation in the complex $Al_{13}Co_4$ alloy during single crystal micropillar compression.

Single crystalline $Al_{13}Co_4$ samples were grown using the Czochralski method. Cylindrical micropillars of dimension 2 μm (diameter) × 5 μm (height) were prepared using focused ion beam (FIB) on a Helios NanoLab under an accelerating voltage of 30 kV and beam currents down to 90 pA. The samples were made from thinned crystals and significant areas behind the pillars were milled out in order to prevent interference of the probe following its exit through the sample in the transmission mode. The vertical pillar axis was parallel to [0 1.174 1], which is 4.6° from the [011]-direction in the orthorhombic crystal. This orientation was so chosen to maximize the Schmid factor on the preferred (001)[010] slip system. *In-situ* micro-Laue diffraction, in transmission, and micropillar compressions were carried out

a)Author to whom correspondence should be addressed. Electronic mail: a.bhowmik@ic.ac.uk

on beamline B16 at the Diamond Light Source, UK.[26] A schematic of the experimental setup is shown in Figure 1. The incident micro-focused "white" x-ray beam, focused using Kirkpatrick-Baez (KB) mirrors, had an energy range of 8–25 keV and spot size of 0.8–1 μm full-width-half-maxima. The diffraction patterns were captured during the test using a large area (3056×3056 pixels, 31 μm pixel size) 16-bit CCD camera (ImageStar 9000 area detector, Photonic Science, Ltd.) recording one pattern every 40 s with exposure time of 10 s. The samples were compressed at loading rate of 0.4 μN s^{-1} using Hysitron compression rig fitted with a flat punch.[20] As a single crystal pillar sample is deformed, due to rotation of the crystal planes and the presence of strain gradients within the unit cells, the shape and position of the diffracted spot changes as shown pictorially in the inset of Figure 1. Post-deformation micrographs of the compressed pillars were obtained using Helios Nanolab 600 SEM. The deformed pillars were cross-sectioned and using the *in-situ* lift-out technique the microstructure of the cross-section was studied using a JEOL 2100F transmission electron microscope (TEM).

The incident beam on the micropillar was parallel to the $[\bar{2}\ \bar{8}\ 7]$ zone axis. The recorded diffraction patterns were captured and contained many reflections, as these CMAs are low symmetry structure with large unit cells. Prior to deformation, the reflections from the micropillar were generally symmetric but appreciable broadening was observed. The width of the reflections at the base was ~0.2° (Figure 2(a)), which is quite substantial compared with instrumental broadening.[21,22] One possibility is that this is caused by FIB milling process that induces prior strain gradient in micropillars due to sputtering and radiation damage, which is dependent on both the size and material of the pillar.[14,15] This existing strain gradient influences plastic deformation of pillars at initial stages and results in an extraneous hardening before slip on predicted slip system can start operating. Pillars were milled with 30 kV ion beam that typically induces 30 nm of damage on the surface skin of a 2 μm diameter pillar.[23] During progressive compression of the pillar, distinct changes in the shapes and positions of the peaks were observed. Figures 2(a)–2(k) show the evolution of the (220)-peak with increasing compressive load until peak load, isolated from the whole Laue diffraction pattern while Figure 2(l) shows the final position of the reflection after unloading. As mentioned earlier, the (220) peak is symmetrical in undeformed micropillar with an intensity spread (Figure 2(a)). As the micropillar was compressed, following an initial period of unchanged peak shape, the reflection moved away from the initial position corresponding to an applied stress of ~600 MPa. Upon continued compression, the Laue peak is observed to simultaneously streak along a well-defined direction (S1 in the supplementary material[24]). The peaks were fitted using a 2D Gaussian function and the centers of the fitted peaks are plotted in Figure 2(m). Assuming considerable friction between the indenter punch and top surface of the pillar, the direction of movement of the Laue spots (i.e., crystal planes) is primarily governed by the rotation of the pillar under constrained compression following Taylor's model.[25] The rotation of the individual peaks is strictly dictated by the activation of specific slip systems in the crystal. Assuming a given slip system, a rotation axis, $\boldsymbol{N}$, and angle, θ, can obtained from the cross product and dot product, respectively, of the known loading direction and slip plane normal. A 3×3 Rodriguez rotation matrix, $\boldsymbol{R}$, can subsequently be generated as follows: $\boldsymbol{R} = \boldsymbol{I} + (\sin\theta)\boldsymbol{N} + (1 - \cos\theta)\boldsymbol{N}^2$, where $\boldsymbol{I}$ is the identity matrix. Considering slip on the (001) plane, this results in a rotation matrix, $\boldsymbol{R} = \begin{bmatrix} 1 & 0 & 0 \\ 0 & 0.706 & -0.708 \\ 0 & 0.708 & 0.706 \end{bmatrix}$. The rotation of a given plane normal, $\hat{n}$, can be obtained by, $\hat{n}_{rotated} = \boldsymbol{R}\hat{n}$. During plastic deformation, rotation of the planes is manifested by gradual rotation of the peaks. This rotation follows the direction corresponding to the operation of a slip system with maximum resolved shear stress. The path of rotation of a given peak depends on the initial orientation of the micropillar. In the case of two competing slip systems, the peak generally follows the resultant path, depending on the time resolution of subsequent images and the loading rate.[17,19] In orthorhombic $Al_{13}Co_4$, the (001)[010] is the preferred slip system. With

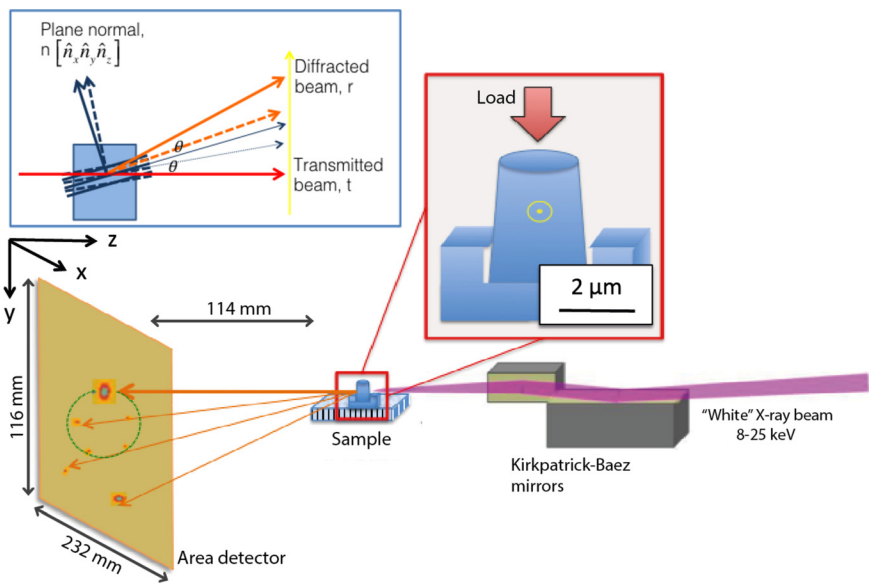

FIG. 1. Schematic representation of the *in-situ* micro-Laue experiment in transmission mode using a "white" x-ray beam. The circled dot denotes the position of the beam on the pillar. A pictorial representation of the principle of Laue diffraction is also shown in the inset describing the movement of diffracted peak upon rotation of crystal planes as a result of deformation. The solid and dotted lines denote the initial and final vectors.

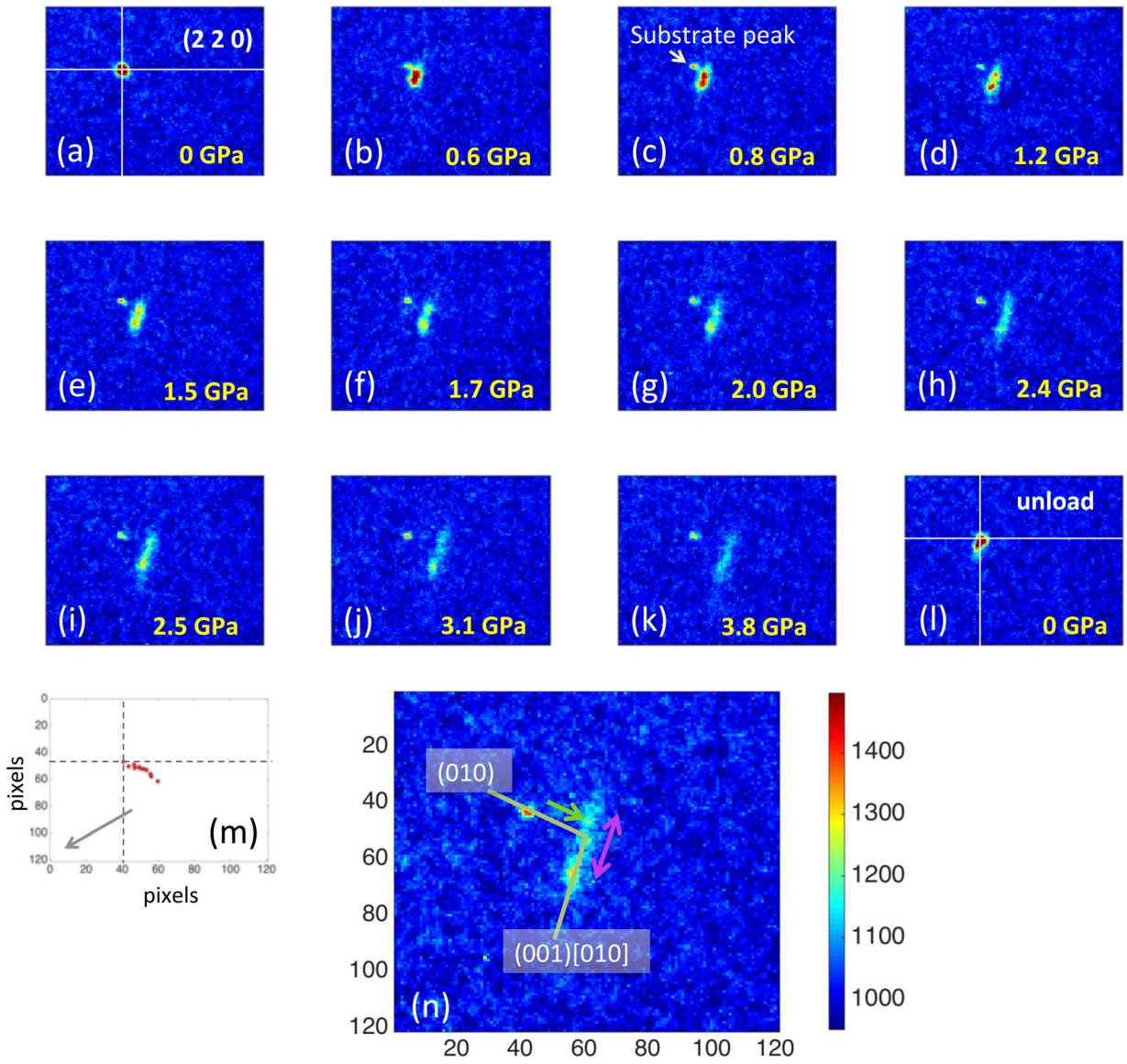

FIG. 2. (a)–(l) Evolution of the (220) reflection with increasing compressive stress showing rotation and streaking of the peak. (m) Legend showing the movement of the peak centres with increasing strain. The arrow points to the direction of the transmitted beam. (n) The streaked reflection on which is superimposed the vectors denoting the direction of rotation and streaking due to the operation of two different slip systems in $Al_{13}Co_4$. The legend in (n) denotes intensity in arbitrary units.

the vertical axis of the pillar parallel to [0 1.174 1], both (001)[010] and (010)[001] slip systems have the same Schmid factor of ~0.5. As shown in Figure 2, the path taken by the centroid of the (220)-reflection corresponds to the rotation of the plane due to activation of slip on the (010) plane. However, during analysis of post-deformed $Al_{13}Co_4$ sample oriented along the [$\bar{6}$ $\bar{4}$ 5] loading direction, Heggen *et al.*[2] observed that planar faults were only associated with (001) planes. No abrupt changes in the path of rotation of the peaks, which might suggest sudden strain bursts within the micropillar, caused by critical slip processes like accumulation of dislocations or activation of a competing slip system, were apparent during compression. This is attributed to the lack of multiple slip systems in $Al_{13}Co_4$ and the greater ease of slip on the primary (001) plane.

The streaking direction is consistent with continuous slip activity on the (001)-plane and storage of dislocations within the illuminated volume, resulting in local strain gradient. The rotation and streaking directions of the peak are marked in Figure 2(n). Preferential streaking of Laue spots implies that scattering from the sample is predominantly caused by the presence of a longer ranged deviatoric strain gradients and lattice rotation gradients in the micropillar. The continual evolution of such gradient could be caused by the generation of excess unpaired geometrically necessary dislocations (GNDs) with increasing compressive strain. The continuous activity of dislocation on the (001)[010] slip system accommodates the strain in the micropillar that eventually led to the formation of a slip step, as shown in Figure 3(a). Calculating the angle of the slipped step with respect to the pillar axis, it is inferred that the slip plane corresponds to the (001) crystallographic plane. The cross-section TEM image of the slipped micropillar is shown in Figure 3(b) with the slipped step clearly visible. The foil is imaged at a tilt angle of ~6° when the foil normal was parallel to the [$\bar{1}$ $\bar{2}$ 2] zone axis. Deformation of the micropillar was accommodated by formation of both stacking faults and dislocations, as seen within the sectioned pillar (Figures 3(c) and 3(d)). Stacking faults are observed to form parallel to the slip step. When viewed under a two-beam condition, with $\mathbf{g} = 2\ 0\ \bar{2}$

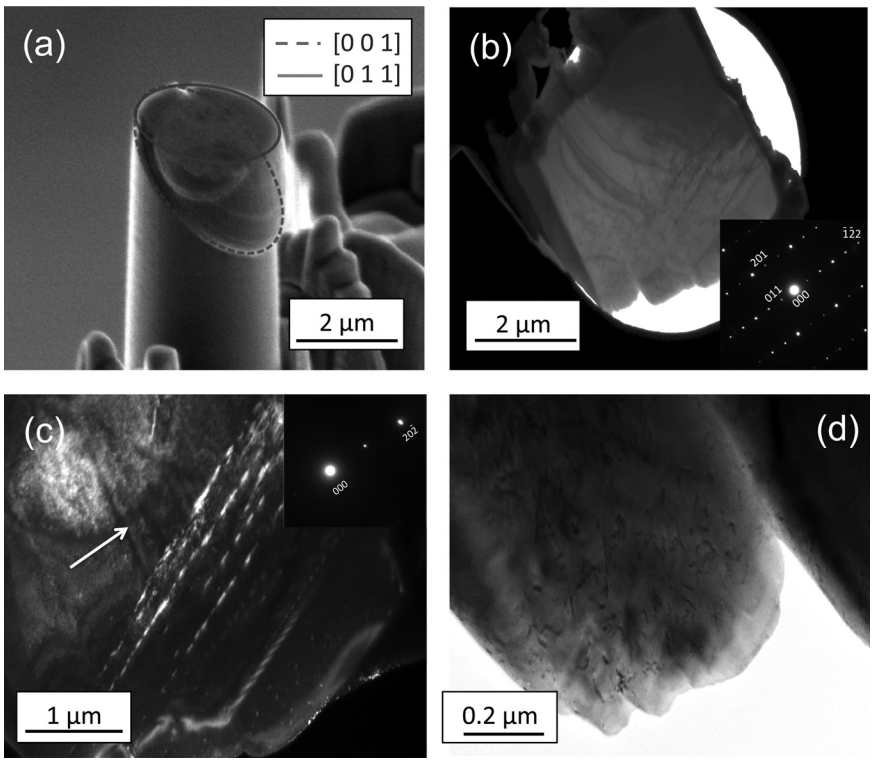

FIG. 3. (a) Post-mortem scanning electron microscope image of the slipped $Al_{13}Co_4$ micropillar showing only one major slip trace on (001) plane. (b) Transmission electron micrograph showing the section of the slipped pillar with the foil normal parallel to the $[\bar{1}\ \bar{2}\ 2]$ zone axis. (c) Dark-field image of stacking faults parallel to the slip direction viewed under $g = 2\ 0\ \bar{2}$ condition, and (d) dislocations within the deformed pillar in the bright field mode.

reflection, the faults were in contrast, indicating that the fault vector is likely to be [001], i.e., the faults lie on the (001) plane. After unloading the pillar, the final peak reverts back to almost the same position but now with noticeable streaking (Figure 2(l)). This is supported by TEM observation of both shearing of the pillar and stacking fault formation.

In bulk samples, the deformation mechanism of $Al_{13}Co_4$ constitutes of pure glide of metadislocations, with [010] Burgers vector on the (001) plane bounded by stacking faults. Increasing deformation leads to increase in densities of both the stacking faults and dislocations.[2] A similar effect is also seen in compression of micropillars that results in the extensive streaking of Laue spots. As mentioned above, straining leads to the generation of geometrically necessary, i.e., unpaired dislocations, in the sample which could rationalise the formation of high density of faults formed in $Al_{13}Co_4$ bound by such unpaired dislocations separated by long distances over the lattice in such low stacking fault energy compounds. The movement of metadislocations within such alloys is a complex process involving the cooperative rearrangement of atoms within its core. The glide of metadislocation is associated with escort (so-called "phason") defects and leaves a monoclinic phase within the orthorhombic tiling in its wake. Within the deformed cross-section of the micropillar, no slip traces on the alternate (010) slip plane was observed in the TEM besides the faults parallel to the (001) plane. Therefore, it is believed that the initial rotation of the reflection is not due to crystallographic slip on the (010) plane but rather due to improper loading of the pillar causing the generation of a bending moment and/or constraint imposed on the pillar due to the pre-existing strain gradient from the FIB milling process. It is observed that the substrate signal remains and that the peak moving away from its initial position must represent the sample. This gives an indication that the sample did not rotate much at all via internal lattice rotation, but that the major part of the peak movement, albeit small, is due to non-plastic processes.

Another feature observed in the Laue spots captured during compression was the splitting of peaks. In Figure 4(a), the (143) reflection shows a split in the streaked peak, which denotes that some of the GNDs tend to rearrange into walls (sub-grain boundaries) while loading. In this case, the two dissociated spots signify that the slipped and unslipped parts are the two independently scattering misorientated sub-volumes within the micropillar. Identical splitting is also observed in (220)-peak, besides streaking (Figure 2), but at stress values of 0.8 GPa (Figure 2(c)), much lower than the reported yield stress of 2 GPa,[8] where the (001)[010] system was aligned for slip—this indicates that slip activity is already initiated at an earlier stage. At 2 GPa stress, significant deformation is already induced in the pillar, visible from the diffused streaking of the peak (Figure 2(g)). The measured misorientation, $\theta = 0.35°$, between the two split spots is related to the lattice curvature and hence the GND density, ρ. This can be estimated using the relations $\frac{b}{h} = 2\sin\theta$ and $\rho = \frac{1}{Dh}$,[26] assuming that the dislocations present lie on the preferred (001)[010] slip system within the probed area D and h is the separation distance of the dislocations. Using Burgers vector, $b = 0.290$ nm in $Al_{13}Co_4$ for this slip system[7] and $D = 2\,\mu$m, the estimated GND density was $1.1 \times 10^{13}\,m^{-2}$. This is approximately same as the dislocation density of $1.4 \times 10^{13}\,m^{-2}$, observed in bulk $Al_{13}Co_4$ deformed at 973 K to a strain of 6.2%.[2] However, it can be seen that the peaks are not distinctly separated but are overlapped. When coherently scattering fragments or sub-grains form due to rearrangement of unpaired dislocations within the sample volume, diffraction of white light from the misorientated sub-volumes causes Laue peaks to split. Simulations showed that overlapping would be observed when only 5%–25% of total dislocation population had formed into sub-

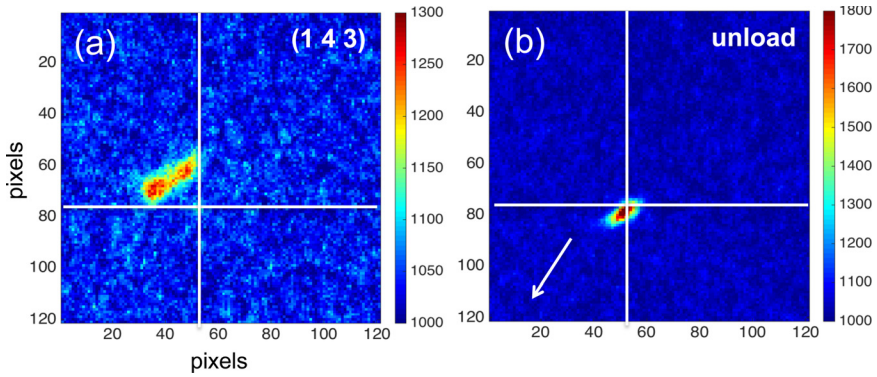

FIG. 4. (a) The (143) reflection in the Laue pattern showing peak split during compressive loading indicative of rearrangement of dislocation network into sub-grain boundaries. (b) The final peak after unloading.

grain boundaries—complete splitting would only occur if at least 75% of dislocations had formed distinct sub-grain boundaries.[26] This observation possibly implies that only a small percentage of overall GNDs form the slipped-unslipped boundary with significant numbers still present within the respective slipped and unslipped volumes as randomly distributed dislocations. After unloading, however, the two split peaks coalesced indicating that the final misorientation in the pillar was insignificant with a reordering of the GNDs within the volume into a slip step. Residual streaking (Figure 4(b), also S2 in the supplementary material[24]) showed remnant plastic strain gradient in the sample volume. This has also been observed in the post-compression microstructure where only random dislocations were found in the sample.

In summary, we have investigated the deformation behaviour of $Al_{13}Co_4$ CMA using micropillar compression combined with *in-situ* transmission micro-Laue diffraction and post-deformation TEM that gave valuable insights into the dynamics of deformation behavior of CMAs. Initial rotation of Laue peaks observed at early stages could have resulted from preexisting strain gradient in the pillar—although the magnitude of the rotation suggested very little lattice rotation in these $Al_{13}Co_4$ CMAs prior to the onset of plasticity. Streaking of the peaks along a preferred direction confirmed the evolution of a deviatoric strain gradient within the sample arising due to continued slip on the (001)[010] system. This resulted in the formation of a slip step in the micropillar as observed in post-deformation TEM. Splitting of peaks into two, indicating formation of misorientated sub-volumes within the pillar, was noted to occur at 0.8 GPa, substantially below the reported overall yield stress of 2 GPa. However, the misorientated sub-volumes relax upon unloading with rearrangement of dislocations.

We appreciate valuable technical input from John Plummer (Imperial College, now with the Nature Publishing group) and Wenjun Liu (34-ID-E, APS). Financial support for the work was provided by the Engineering and Physical Sciences Research Council (EP/K028707/1). We thank Diamond Light Source for access to beamline B16 (MT8179) that contributed to the results presented here, and Andrew Malandain for technical support. In addition, preliminary research used resources of the Advanced Photon Source (34-ID-E, John Tischler), a U.S. Department of Energy (DOE) Office of Science User Facility operated for the DOE Office of Science by Argonne National Laboratory under Contract No. DE-AC02-06CH11357; as well as beam-time at the Advanced Light Source (12.3.2), supported by the Director, Office of Science, Office of Basic Energy Sciences, of the U.S. Department of Energy under Contract No. DE-AC02–05CH11231. W.J.C. and N.G.J. were supported by the EPSRC-Rolls-Royce Strategic Partnership (EP/M005607/1 & EP/H500375/1). T.B.B. is supported by a research fellowship from RAEng. The raw data for reproducing figures presented in the paper can be found at https://zenodo.org/record/47061.

[1]J. Grin, U. Burkhardt, M. Ellner, and K. Peters, J. Alloys Compd. **206**, 243 (1994).
[2]M. Heggen, D. Deng, and M. Feuerbacher, Intermetallics **15**, 1425 (2007).
[3]H. Klein, M. Feuerbacher, P. Schall, and K. Urban, Phys. Rev. Lett. **82**, 3468 (1999).
[4]M. Heggen and M. Feuerbacher, Acta Mater. **61**, 3851 (2013).
[5]M. Heggen, L. Houben, and M. Feuerbacher, Nat. Mater. **9**, 332 (2010).
[6]M. Heidelmann, M. Heggen, C. Dwyer, and M. Feuerbacher, Scr. Mater. **98**, 24 (2015).
[7]M. Heggen and M. Feuerbacher, Mater. Res. Lett. **2**, 146 (2014).
[8]C. Walter, J. M. Wheeler, J. S. Barnard, R. Raghavan, S. Korte-Kerzel, P. Gille, J. Michler, and W. J. Clegg, Acta Mater. **61**, 7189 (2013).
[9]G. E. Ice and J. W. L. Pang, Mater. Charact. **60**, 1191 (2009).
[10]F. Hofmann, X. Song, I. Dolbnya, B. Abbey, and A. M. Korsunsky, Procedia Eng. **1**, 193 (2009).
[11]B. C. Larson, W. Yang, G. E. Ice, J. D. Budai, and J. Z. Tischler, Nature **415**, 887 (2002).
[12]L. Margulies, G. Winther, and H. F. Poulsen, Science **291**, 2392 (2001).
[13]R. Maaß, S. Van Petegem, D. Ma, J. Zimmermann, D. Grolimund, F. Roters, H. Van Swygenhoven, and D. Raabe, Acta Mater. **57**, 5996 (2009).
[14]R. Maaß, S. Van Petegem, C. N. Borca, and H. Van Swygenhoven, Mater. Sci. Eng., A **524**, 40 (2009).
[15]J. Zimmermann, S. Van Petegem, H. Bei, D. Grolimund, E. P. George, and H. Van Swygenhoven, Scr. Mater. **62**, 746 (2010).
[16]C. Kirchlechner, P. J. Imrich, W. Grosinger, M. W. Kapp, J. Keckes, J. S. Micha, O. Ulrich, O. Thomas, S. Labat, C. Motz, and G. Dehm, Acta Mater. **60**, 1252 (2012).
[17]C. Marichal, H. Van Swygenhoven, S. Van Petegem, and C. Borca, Sci. Rep. **3**, 2547 (2013).
[18]R. Barabash, G. E. Ice, B. C. Larson, G. M. Pharr, K.-S. Chung, and W. Yang, Appl. Phys. Lett. **79**, 749 (2001).
[19]R. Maaß, S. Van Petegem, H. Van Swygenhoven, P. M. Derlet, C. A. Volkert, and D. Grolimund, Phys. Rev. Lett. **99**, 145505 (2007).
[20]H. E. Weekes, V. A. Vorontsov, I. P. Dolbnya, J. D. Plummer, F. Giuliani, T. B. Britton, and D. Dye, Acta Mater. **92**, 81 (2015).
[21]R. Maaß, S. Van Petegem, J. Zimmermann, C. N. Borca, and H. Van Swygenhoven, Scr. Mater. **59**, 471 (2008).
[22]R. Maa*β*, D. Grolimund, S. Van Petegem, M. Willimann, M. Jensen, H. Van Swygenhoven, T. Lehnert, M. A. M. Gijs, C. A. Volkert, E. T. Lilleodden, and R. Schwaiger, Appl. Phys. Lett. **89**, 151905 (2006).
[23]W. J. MoberlyChan, D. P. Adams, M. J. Aziz, G. Hobler, and T. Schenkel, MRS Bull. **32**, 424 (2007).
[24]See supplementary material at http://dx.doi.org/10.1063/1.4944486 for the response of different peaks during compression of the $Al_{13}Co_4$ micropillar.
[25]W. F. Hosford, *The Mechanics of Crystals and Textured Polycrystals* (Oxford University Press, New York, 1993).
[26]R. I. Barabash, G. E. Ice, and F. J. Walker, J. Appl. Phys. **93**, 1457 (2003).